Journal of The
Electrochemical Society



# On the Proposed Mechanism of Transpassive Film Formation in Pure Ni in Sulfate Environment: Insights from In Situ Raman Spectroscopy and Respirometry

To cite this article before publication: Karthikeyan Hariharan *et al* 2026 *J. Electrochem. Soc.* in press https://doi.org/10.1149/1945-7111/ae3b17

# On the Proposed Mechanism of Transpassive Film Formation in Pure Ni in Sulfate Environment: Insights from In Situ Raman Spectroscopy and Respirometry

| | |
|---|---|
| Journal: | *Journal of The Electrochemical Society* |
| Manuscript ID | JES-115659.R1 |
| Manuscript Type: | Research Paper |
| Date Submitted by the Author: | 14-Jan-2026 |
| Complete List of Authors: | Hariharan, Karthikeyan; Friedrich-Alexander University Erlangen-Nuremberg, Materials Science and Engineering<br>Kosanam, Koushik; Friedrich-Alexander University Erlangen-Nuremberg, Materials Science and Engineering<br>Götz, Carina; Forschungszentrum Jülich GmbH, Helmholtz Institute Erlangen-Nuremberg for Renewable Energy (IEK-11); Friedrich-Alexander-Universitat Erlangen-Nurnberg, Department of Chemical and Biological Engineering<br>Bruns, Mark; University of Erlangen-Nuremberg, Department of Materials Science, WW-4<br>Böhm, Thomas; Forschungszentrum Jülich GmbH, Helmholtz Institute Erlangen-Nuremberg for Renewable Energy (IEK-11)<br>Marcus, Philippe; PSL Research University,<br>sridhar, narasi; The Ohio State University, Materials Science & Engineering<br>Virtanen, Sannakaisa; Friedrich-Alexander-University of Erlangen-Nürnberg, Materials Science, WW-4 |
| Keywords: | Ni, OER, Raman spectroscopy, Respirometry, transpassive film, transpassivity |
| | |

# On the Proposed Mechanism of Transpassive Film Formation in Pure Ni in Sulfate Environment: Insights from In Situ Raman Spectroscopy and Respirometry

Karthikeyan Hariharan,[1,*,a,z] Koushik Kosanam,[1] Carina Götz,[2,3] Mark P. Bruns,[1] Thomas Böhm,[3] Philippe Marcus,[4,**] Narasi Sridhar,[5,*] and Sannakaisa Virtanen[1,**,z]

[1]Friedrich-Alexander-Universität Erlangen-Nürnberg, Department of Materials Science & Engineering, Institute IV: Surface Science and Corrosion (LKO), Erlangen 91058, Germany

[2]Department of Chemical and Biological Engineering, Friedrich-Alexander-Universität Erlangen-Nürnberg, 91058 Erlangen, Germany

[3]Helmholtz Institute Erlangen-Nürnberg for Renewable Energy (IET-2), Forschungszentrum Jülich, 91058 Erlangen, Germany

[4]PSL Research University, CNRS - Chimie ParisTech, Institut de Recherche de Chimie Paris (IRCP), Physical Chemistry of Surfaces Group, Paris 75005, France

[5]Fontana Corrosion Center, Department of Materials Science and Engineering, The Ohio State University, Columbus 43210, United States

*Electrochemical Society Member.

**Electrochemical Society Fellow.

[a]Present address: Corrosion Metallurgy Laboratory, Department of Metallurgical Engineering and Materials Science, Indian Institute of Technology Bombay, Mumbai 400076, India.

[z]E-mail: karthik.hariharan@iitb.ac.in;sannakaisa.virtanen@fau.de

## Abstract

A mechanism for transpassive film formation in pure Ni in a sulfate environment is proposed based on *in situ* Raman spectroscopy and electrochemistry-coupled respirometry. Based on potentiostatic respirometry on pure Ni in 0.1 M $K_2SO_4$, there is a characteristic time-delay before the onset of oxygen evolution, coinciding with the onset of transpassive film formation upon stepping the potential from passive into the transpassive regime. At the same time, *in situ* Raman spectroscopy revealed that the transpassive film comprised of NiOOH. It reduced back without any time-delay after returning to open-circuit conditions to a passive $Ni(OH)_2$.

## Introduction

The transpassive regime in metals and alloys is complicated to decipher using only conventional electrochemical testing methods, since it is a dynamic phenomenon involving several reactions such as metal dissolution, transpassive film formation, and water oxidation, occurring simultaneously at the metal(oxide)/electrolyte interface. Therefore, it becomes essential to use operando surface analytical

measurements with methods such as surface-enhanced Raman spectroscopy [1, 2], ambient pressure X-ray photoelectron spectroscopy [3, 4], X-ray absorption near-edge spectroscopy [5-7], *in situ* reaction monitoring methods like respirometry [8] and solution analysis like inductively coupled plasma-atomic emission spectroscopy[9], together with electrochemical tests to gain a phenomenological understanding of elementary processes governing transpassive behavior of metals and alloys.

Cr-passivated Fe and Ni-based alloys hold significant industrial importance as corrosion-resistant structural materials. They are valuable candidates for investigating transpassive corrosion mechanisms, since they are considered suitable for applications such as fuel cells/electrolyzers bipolar plates[10-12] and nuclear waste reprocessing plants[13-15], where they can encounter transpassive conditions. Furthermore, there exists a substantial body of knowledge within this alloy system that can be further expanded. For instance, the behavior of Cr in transpassive regime is well-understood. It is an established fact that Cr undergoes oxidative dissolution from Cr(III) oxide to soluble Cr(VI) species [7]. However, it is equally important to clarify the role of other constituent elements, namely Fe and Ni. There are some studies claiming the positive role of Fe in improving resistance in the transpassive regime through an Fe(III) based transpassive film [16]. Still, Ni transpassivity remains elusive, partly due to contradictory findings over the years about the interplay between water oxidation, dissolution, and transpassive film formation[17, 18]. Therefore, it is necessary to study the behavior of pure Ni because the behavior of alloys is strongly influenced by the behavior of the constituent elements and their interactions.

In our preceding work [8], we used electrochemistry-coupled respirometry measurements on pure Ni in 0.5 M $Na_2SO_4$ at pH = 5 to, in principle, demonstrate the utility of non-electrochemical tools, and to answer some of the mechanistic questions in transpassivity. In that work, it was shown that the oxygen evolution reaction (OER) induced acidification did not trigger transpassive dissolution. The findings were in contrast with previous studies that attributed OER as the causal factor triggering transpassivity in Ni[18, 19]. Furthermore, it was shown that the OER onset coincided with an arrest in dissolution charge density, which was attributed to the formation of Ni (III) transpassive film (NiOOH), a known OER electrocatalyst[20-22]. However, due to the innate transient nature of Ni (III) species in the absence of a potential control, direct evidence was not provided. Furthermore, we also did not provide a mechanism for transpassive film formation. Especially, the physical basis of time-delay for OER onset/transpassive film formation, when stepped to the transpassive range from the passive range in potentiostatic respirometry, was left unexplored in detail. In the current study, we probe the transpassive film formation using operando measurements with Raman spectroscopy and additional potentiostatic respirometry experiments to propose a mechanism for transpassive film formation.

## Experimental

*Specimen and electrolyte description*

In this work, high-purity 99.9+% Ni (CHEMPUR Feinchemikalien und Forschungsbedarf GmbH, Karlsruhe, Germany) was used as-received in bright annealed condition. The Ni was supplied in the form of 0.125 mm thick foil, which was cut to an approximate area of 1 $cm^2$. To establish electrical contact, the specimen was spot-welded to a 304 stainless steel wire. Subsequently, the specimens were coated with a blue lacquer, encompassing the welded stainless steel wire, allowing room only for the tip to be inserted into the connection plug as shown in Figure 1a. This coating process was designed to control the exposed area of Ni and allowed to dry overnight. The samples are cleaned with DI water before testing. The exposed area among specimens was measured using ImageJ software for all specimens. The exposed areas varied between 0.02 to 0.1 $cm^2$.

All measurements in this study were conducted in 0.1 M $K_2SO_4$ solution, no additional deaeration was carried out. The pH of the solution was adjusted by adding appropriate quantities of $H_2SO_4$ until the pH = 5. Since we did not use a buffer, the pH adjustment was carried out only prior to the actual measurement to maintain a constant pH at the start of the experiment. The pH was measured every time before each measurement using a SevenCompact™ pH/Cond meter (Mettler-Toledo GmbH, Germany). The choice of sulfate electrolyte and the pH of 5 was to maintain consistency with our previous work. However, we changed the cation to $K^+$ compared to $Na^+$, since we intend to study different Ni/Fe alloys in future work on alloy dissolution, necessitating ICP-MS measurements that are affected by $Na^{+23}$. The sulfate concentration was changed to 0.1 M from 0.5 M in the previous work, to slow down dissolution and prevent the thin Ni foil from being fully consumed during the *in situ* Raman measurement.

*Standalone electrochemical-respirometric measurements*

All the measurements were done with a PalmSens 4 potentiostat (PalmSens BV, The Netherlands) in a 3-electrode cell with Ag/AgCl (satd. KCl) reference electrode, and Pt counter electrode. The Pt counter electrode was placed in a separate chamber that was attached to the main compartment and ionic transport was ensured through a Nafion™ membrane, but there was no gas/electrolyte flow between the two chambers. The Ag/AgCl reference electrode was also placed in a separate compartment, a connection was made to the main compartment through a 304L stainless steel metal bridge, whose utility was demonstrated by Choudhary et al.[24] – this was done to avoid chloride contamination in the working electrode compartment. The manometric electrochemical-respirometric setup was described in our previous work, the schematic is reproduced here for reference in Figure 1b. Two commercial $O_2$ sensors (PyroScience GmbH, Germany) were used to monitor changes in $O_2$ in the electrolyte and the headspace, respectively. The PyroScience $O_2$ sensors work based on oxygen-induced quenching due to inelastic scattering[25]. The sensor consists of a luminophore and uses red LED light as a light source. When the luminophore gets excited by the red LED light and it returns to the ground state by emitting luminescence. However, when oxygen molecules collide with the excited luminophore, it promotes non-radiative energy transfer through inelastic scattering resulting in a decrease of emitted light intensity. The sensor quantifies this change in intensity and converts it into an electrical signal using Stern-Volmer relationship. The accuracy of the $O_2$ sensor, as specified by the manufacturer is ± 2 hPa (2 millibar) for the gas-phase sensor and 0.1 mg/L electrolyte phase sensor. The resolution for gas and liquid phase

sensors are 0.5 hPa and 0.025 mg/L respectively. The detection limits for gas and liquid phase sensors are 0.2 hPa limit and 0.01 mg/L respectively. The sensor spots were calibrated using a 2-point calibration procedure, with the 0 % factory calibration taken as the default first point and the actual test conditions being the second point following the PyroScience Oxygen sensor's manual [25]. The rapid response time of the oxygen sensor was demonstrated by Xie et al.'s recent work[26], which used galvanostatic pulse experiments on Pt (a known electrochemical system with 100% anodic charge coming from OER) to confirm that the respirometric sensing of Oxygen was real-time and any time-delay in oxygen evolution is physical and not due to the slow response of the sensor.

Firstly, all the experiments had 1 h long open circuit potential (OCP) holds before the measurement to ensure a reasonable steady state, followed by potentiostatic holds at 0.2 V (vs. Ag/AgCl) in passive regime for 30 min and 1.5 $V_{Ag/AgCl}$ or 2 $V_{Ag/AgCl}$ in the transpassive range for 30 min. Measurements were repeated three times to ensure that the observed behavior is representative of the material behavior. To account for the anodic charge contributions from dissolution and the OER, the oxygen sensor data from both the electrolyte phase as well as headspace were converted into number of moles of $O_2$ and added together. Subsequently, the total number of moles were converted to charge through Faraday's law. The dissolution charge was inferred by subtracting the oxygen charge from the total electric charge (measured by the potentiostat). While the oxygen concentration was continuously monitored in real-time, the cathodic oxygen charge at OCP, which corresponds to the oxygen reduction reaction, was subtracted from the data to bring the OER charge density to zero at the point of OER onset.

*In situ Raman spectroscopy measurements*

*In situ* Raman spectroscopy measurements were performed using a WITec alpha 300 RA (WITec, Germany) confocal Raman microscope with a laser wavelength of 785 nm, operating at an intensity of 72 mW, using a Zeiss LD EC Epiplan–Neofluar 50x/0.55 objective (Zeiss, Germany) to focus on the sample surface. The Raman signal was detected using a WITec UHTS 300 VIS-NIR spectrometer (WITec, Germany) with a Peltier-cooled back-illuminated EMCCD camera and a 300 grooves $mm^{-1}$ optical grating. The integration time for each spectrum was 10 s with a number of accumulations of 10. The schematic of electrochemical cell with a 3-electrode setup shown in Figure 1c, was used for the Raman measurements. Figure 1d shows the image of the electrochemical cell designed to make it fit within the platform of the microscope. Sample inside the working compartment is positioned in a way that the exposed area of sample is within the exposed window for Raman spectroscopy. Then the Raman microscope is focused on to the exposed area of sample within exposed window. The electrochemical sequence was adjusted as follows to reduce the time at the Raman microscope – it involved 30 min OCP, followed by a 30 min hold at 0.2 $V_{Ag/AgCl}$ and finally a 15 min hold at 1.5 $V_{Ag/AgCl}$.

The cell body (cuvette) was made of Schottglas B270® (Schott AG, Germany) to ensure good transmission of light for the Raman measurements. The fluorescent background of the Raman spectra

was removed using the shape-based background subtraction algorithm from the software WITec project FIVE+ (WITec, Germany) at a shape size of 1000. Each spectrum was smoothened by a moving average over 5 data points and subsequently normalized to its maximum peak height. Due to the complexity of the *in situ* Raman spectroscopy measurements, only one Ni sample was investigated.

## Results and Discussion

*Potentiostatic respirometry at +1.5 $V_{Ag/AgCl}$*

In Figure 2a, the log current density vs. log time plot shows the expected passive behavior of Ni with typical decay due to passive film growth. The plot in Figure 2b is consistent with the transpassive behavior. Figure 2c shows the representative charge density vs. time plot, showing the measured OER charge density, total charge density, and the inferred dissolution charge density at different applied potentials. In the passive range (at +0.2 $V_{Ag/AgCl}$), the total charge stays low with no sign of OER, as expected. When the potential is jumped to +1.5 $V_{Ag/AgCl}$ into the transpassive regime, the total charge density (from the potentiostat) increases immediately, but no oxygen signal is measured until 7.8 min after the potential step. Based on three repeats, the time-delay for OER onset was 6 $\pm$ 1.3 min. The time-delay is physically meaningful and not due to slow sensor response in detecting oxygen, as the ability of the respirometry method and the oxygen sensor response time has been established in earlier works and would not significantly contribute to the here observed time-delay [27-30]. Moreover, it is also consistent with the findings of our previous work on Ni transpassivity, where there is a consistent time-delay before OER onset, and dissolution accounts for the entire anodic charge.

It is important to discuss the sudden upward jumps in the $Q_{OER}$ (also showing up as sudden drops in dissolution); these are due to $O_2$ bubble nucleation and their release into the cell headspace. This occurs because we have no external stirring, coupled with a low rate of bubble nucleation at potentials close to the OER onset potential for Ni (+1.3 $V_{Ag/AgCl}$, refer to Figure S1 supplementary materials). As it will be shown later in the paper, at hold potentials considerably above the OER onset potential (e.g. at +2 $V_{Ag/AgCl}$), this artifact will vanish due to higher bubble nucleation rates, creating an effect like that of external stirring. While this artifact can affect the accuracy of the instantaneous value of $Q_{OER}$ and $Q_{dissolution}$ in the near $O_2$ saturated condition, this will not interfere with our determination of the initial time-delay for OER onset. This assumption is reasonable because we are at around 80% of oxygen saturation in the early stages of water oxidation. Consequently, at the OER onset, initially formed $O_2$ molecules would not saturate the electrolyte. Even in the absence of a deaeration step prior to the experiments, the OCP hold for 1 h in a hermetically sealed cell served as a proxy to deaeration as the ORR consumed the dissolved oxygen.

Furthermore, as we are measuring cumulative OER charge and dissolution, it is expected that these parameters monotonically increase over time or remain flat, but the OER charge density data shows fluctuations in Figure 2c (noise). This behavior can be attributed to the way in which the OER charge density is measured. The in situ $O_2$ –sensor monitors the pressure change in the headspace as well as the $O_2$ concentration in the electrolyte continuously. There are small fluctuations (noise) in the sensor

reading influenced by factors including minor changes in temperature. Since the pressure changes and concentration changes are converted to the number of $O_2$ molecules and subsequently to OER charge density via Faraday's law, there are small fluctuations in the OER charge density. Furthermore, the dissolution charge density is inferred by subtracting the OER charge density from the total charge density – therefore the fluctuations also show up in that plot. Nevertheless, the trendline is always increasing/flattening out, consistent with the expected behavior of the cumulative anodic charge plots.

*in situ* Raman spectroscopy during potentiostatic polarization

Figure 3a shows *in situ* Raman spectra of Ni under different polarization conditions, such as at the open circuit potential (OCP), passive regime (+0.2 $V_{Ag/AgCl}$), transpassive regime (+1.5 $V_{Ag/AgCl}$) – spectra collected after ~10 min after the potential jump, and final end-of-test (EOT) at OCP. In addition, Raman spectra of the blue lacquer coating on the sample and the electrolyte, are also shown for decoupling the sample signal from other effects. The spectra for the electrolyte, and blue lacquer were collected outside the test cell (cuvette).

The Raman spectra corresponding to the OCP and the passive states (+0.2 V) do not produce any discernible difference from the electrolyte spectrum. It is because the Raman spectroscopy technique is not sensitive to the ultra-thin passive film (~few nm) that forms under these conditions. However, we know that the surface is passivated under these conditions based on the consistently low current density in the order of mA to nA.cm$^{-2}$. Based on extensive prior literature, the passive film formed on Ni in sulfate environment has a bilayer structure with an outer $Ni(OH)_2$ layer with a NiO inner layer [31, 32]. Furthermore, the outer $Ni(OH)_2$ layer has also previously been reported in Surface Enhanced Raman Spectroscopy (SERS) measurements [1]. It is worth mentioning that even though Ni is not spontaneously passive (i.e. at OCP) in the acidic pH range, we observe spontaneous passive behavior (Figure S2). This can be explained when we consider that Ni can form a very thin film comprising both NiO and $Ni(OH)_2$ in atmospheric air [33], before being exposed to an electrolyte. It is not possible to remove this film [32], except through exposure to an acidic environment with very low pH (such as, concentrated sulfuric acid) or high anodic potentials (in the transpassive regime). In this study, the passive film formed at OCP and low applied potentials is considered to be a baseline to understand the changes occurring at transpassive potentials.

Therefore, it is noteworthy that a potential step to +1.5 $V_{Ag/AgCl}$ into the transpassive regime causes observable changes in the spectrum. Three new peaks appear at 431 cm$^{-1}$, 587 cm$^{-1}$, and 1045 cm$^{-1}$. The twin peaks at 431 cm$^{-1}$ and 587 cm$^{-1}$ are consistent with the signature of the NiOOH formation, as previously reported in the literature[1, 34]. This provides direct evidence that a NiOOH film formed in the transpassive regime. Since the nature of the original passive film comprising of $Ni(OH)_2$/NiO is well-established in the literature, NiOOH has formed likely due to the oxidation of $Ni(OH)_2$, even though we did not directly establish the presence of $Ni(OH)_2$ in the passive regime using Raman spectroscopy. The peak at 1045 cm$^{-1}$ can be inferred to likely arise an adsorbed $HSO_4^-$ species that is stabilized by the OER-driven acidification[35]. However, it does not rule out the probability of the said peak being from sulfate species. This is because $HSO_4^-$ becomes the dominant species only at pH values below 1.5

for the given sulfate concentration, but in our case, while we know OER acidifies the local environment, we do not know the exact local interfacial pH.

After the 15 min hold at +1.5 $V_{Ag/AgCl,}$ the potential control was released, bringing the system back to the OCP, and the EOT Raman spectrum is similar to the initial OCP spectrum. Based on this, it can be inferred that NiOOH is potentially reduced back to $Ni(OH)_2$, while the Ni-sulfate layer (if present) dissolved away. The observation is consistent with the expectation that a NiOOH film (i.e., Ni(III)) is a transient species that can be detected only with a real *in situ* measurement. For example, Boucherit et al. have shown that a NiOOH transpassive film (possibly doped with Fe) formed on Fe-50Ni alloy polarized at +520 mV (vs. $Hg/HgSO_4$) vanished upon removing the potential control during *in situ* Raman spectroscopy measurements in a concentrated KOH solution [36]. The peak at 1045 $cm^{-1}$ vanishing at EOT conditions does not rule out the formation of $HSO_4^-$, as the extent of local acidification decreases after we remove the potential control, potentially destabilizing $HSO_4^-$. In our previous study on Ni transpassivity, the bulk volume of electrolyte was acidified (pH = 2) up to 1 h at OCP after the transpassive hold [8]. However, a pH < 2 is required for the detection of the $HSO4^-$ band at 1045 $cm^{-1}$.

Thus far in the discussion, we have not addressed the presence of a peak at 1249 $cm^{-1}$, which appears under all conditions. While we do not know the exact origin of this peak, it is not from the sample, as it could be seen when we focus far away (0.5 mm) from the sample surface. Since it is confirmed that the peak is not originating from the sample surface, it will not be discussed further in this study.

The results presented so far in Figure 3a confirms that the transpassive film formed on Ni in 0.1 M $K_2SO_4$ at pH = 5 is NiOOH, consistent with previous studies probing transpassive film in different environments including acidic sulfates[37], and boric borate buffer (pH = 8.4)[1]. However, previous work did not discuss the NiOOH formation contextualized based on the repeatable time-delay observed in respirometry measurements. Figure 3b presents Raman spectra collected at three different times – the signatures of NiOOH as well as the adsorbed $HSO_4^-$ do not appear in the spectra collected ~ 1 min after the potential jump to +1.5 $V_{Ag/AgCl}$, and the one collected after ~5 min into the transpassive potentiostatic hold. The signature peaks appear only after ~10 min, which is close to the range of time-delay for OER measured using respirometry under the same electrochemical conditions, showing a clear correlation between OER time-delay observed in respirometry measurements and NiOOH transpassive film formation time-delay seen from the *in situ* Raman spectroscopy measurements.

*Proposed mechanism of transpassive film formation*

Based on the results of in situ Raman spectroscopy and respirometry measurements together with prior literature on the nature of transpassive film, we propose a mechanism of transpassive film formation, wherein the time-delay can be explained on the basis of a sulfate salt-film formation, which shifts the local equilibrium at the salt-film/ transpassive film interface to promote NiOOH formation, which subsequently triggers OER (Figure 4).

The results of our Raman spectroscopy did not show direct confirmation for the sulfate salt-film, and only the presence of an adsorbed $HSO_4^-$ that was stabilized under acidified conditions could be established. However, we hypothesize the necessity of salt-film in the below proposed mechanism to explain the mass-transport limitation (time-delay) as well as the proton migration required for NiOOH film stabilization. Moreover, the hypothesis about the sulfate salt-film mass-transport barrier is not negated by the presence of $HSO_4^-$ detected by the Raman spectroscopy, since the $HSO_4^-$ enrichment at surface was also expected to occur during anodic dissolution of Fe under mass-transport control in presence of a porous film or colloidal dispersion of sulfate products in sulfuric acid[38]. Moreover, the presence of sulfate in the transpassive film of Ni is not unprecedented, as it was reported, for example, by Melendres and Tani in 14 N $H_2SO_4$ based on *ex situ* Raman spectroscopy [39]. This work claimed that there was no oxide/hydroxide in the film, which could be due to the large thickness of the sulfate product, blocking any signal from an underlying oxide/hydroxide film. Moreover, as it was *ex situ* measurement, it is not possible to decouple the salt film formed during the polarization from salt precipitation during drying. However, Delichere et al. suggested formation of Ni sulfate during *in situ* Raman measurements in sulfuric acid [40], but the authors suggested that it was hard to distinguish the sulfate peaks from sulfuric acid due to considerable peak overlap, similar to our case.

In Figure 4a, we represent the situation at OCP and passive state, where a thin bilayer passive film exists, while dissolution of Ni continues to account for considerable anodic charge, albeit at a slow rate. Figure 4b shows the condition in the immediate aftermath of stepping the potential into the transpassive regime prior to OER onset ($t < t_{threshold}$), where the rate of dissolution of Ni has enhanced without any significant changes to passive layer characteristics. At this stage, the concentration of Ni ions at the oxide/electrolyte interface ($C_{surf}$) is well-below the saturation concentration ($C_{sat}$) for a Ni-sulfate formation. In Figure 4c, we reach a stage, $t = t_{threshold}$, where the $C_{surf} = C_{sat}$, a porous hydrated Ni-sulfate salt-film forms above the existing passive layers. Once the salt-film has formed at $t = t_{threshold,+}$ (moments after salt-film precipitation), it triggers the oxidation of $Ni(OH)_2$ and leads to formation of NiOOH, as depicted in Figure 4d. The inner NiO layer could also oxidize to $NiO_x$ [37], but it is not possible to ascertain with the existing results.

A question arises on how the salt-film formation triggers NiOOH oxidation; to answer this, we consider the results of Beck about passivation of Fe under salt-film in acidic sulfate solutions [41]. It was suggested that pores in the salt-film facilitated field-assisted transport of protons away from the salt/metal interface, bringing the local pH conducive for transpassive film formation. We posit a similar possibility of protons being transported from the hydroxide/salt-film interface. However, we rationalize how proton transport away from the interface aids in NiOOH formation through the well-known Le Chatelier's principle [42]. Let us consider the proposed reaction for the oxidation of $Ni(OH)_2$ into NiOOH in the acidic environment:

$$Ni(OH)_2 = NiOOH + H^+ + e^- \quad (1)$$

If the salt-film takes away the protons from the reaction front (i.e. the hydroxide/salt-film interface), then the equilibrium shifts towards the right-hand side of the Eq. (1) and we can predict a higher

thermodynamic driving force for NiOOH formation. Alternatively, we could consider that the proton transport increases the local pH of the reaction front, the reversible potential of Eq. (1) will decrease with an increase in pH according to Nernst's Equation. Since we are holding the potential constant, the overpotential (or the driving force) increases with time as pH increases with time.

This explanation should be applicable for transpassive film formation in the alkaline medium, since the reaction for NiOOH formation in the alkaline medium is written as:

$$Ni(OH)_2 + OH^- = NiOOH + H_2O + e^- \quad (2)$$

In this case, if the potential gradient within the salt is such that $H^+$ (cation) is transported away, then the same potential gradient can transport the $OH^-$ into the reaction interface. If the local $OH^-$ concentration rises due to the presence of a salt-film, then the driving force for NiOOH formation will be increased. While we did not investigate the effect of higher pH in detail, the presence of time-delay during potentiostatic-respirometry is also seen on pure Ni tested at pH = 8 in the same environment (as seen in Figure S3, in supplementary material).

We wish to further elucidate the validity of the proposed mechanism through an additional potentiostatic respirometry experiment at a higher anodic potential (i.e. +2 $V_{Ag/AgCl}$). If the salt-film is indeed driving the NiOOH film formation, then the time-delay should decrease when we hold a higher anodic potential, since the dissolution rate will be greater at 2 $V_{Ag/AgCl}$ than at 1.5 $V_{Ag/AgCl}$ and saturation can be attained faster than at lower potentials. Moreover, the presence of a time-delay at very high anodic potentials will provide indirect evidence for the necessity of the salt-film before the OER onset can occur on Ni.

Figure 6 shows the potentiostatic respirometry with transpassive hold at + 2 $V_{Ag/AgCl}$ after a 30 min passivation at +0.2 $V_{Ag/AgCl,}$ and 1 h at OCP. In Figure 5a and 5b, the current density values in both passive and transpassive regions appear reasonable and consistent with the expectation. Figure 5c, showing the representative charge density vs. time plot, records the time-delay of ~2 min from the time of stepping up the potential to +2 $V_{Ag/AgCl.}$ Based on the replicates, the delay is repeatable with average time-delay of 1.6 $\pm$ 0.6 min, the time-delay is significantly higher than the response time of the sensor and therefore, physically meaningful.

Figure 6 plots the time-delay as function of applied transpassive hold potential, showing an overall decreasing trend. When viewed from the lens of the proposed mechanism of transpassive film formation, the trend in Figure 4 can be interpreted as higher dissolution at higher anodic potential that aids in reaching the $C_{sat}$ earlier and promoting secondary passivity. Moreover, it also confirms the need to have a time-delay, and consequently a salt-film for the formation of transpassive film and OER to occur on the Ni surface.

The fate of salt-film after the transpassive film (NiOOH) formation, during the continued potentiostatic hold in the transpassive regime (after OER onset) was not addressed in the discussion of proposed mechanism in Figure 4. However, it is essential to contemplate the fate of salt-film after the transpassive film formation, since we draw analogy to passivation of Fe under the salt-film, where the

salt-film dissolves away after the passive film forms underneath it. On the other hand, in case of the transpassive film on Ni, the oxyhydroxide film is not as protective as a "real" passive film[43] and allows significant dissolution to take place, as evident from Figure 2b. Therefore, the salt-film could remain above the NiOOH surface, if the dissolution maintains the salt/transpassive film interfacial metal cation concentration at $C_{sat}$. At the same time, there is no question of salt-film remaining intact once the potential control is removed and the potential returns to OCP, as the transpassive film reduces back into a relatively protective passive film and the dissolution is no longer sufficient to maintain the saturation of metal cations at the surface.

*Potential limitations and outlook*

The mechanism of transpassive film formation of Ni underneath a salt-film shown to be operative in 0.1 M $K_2SO_4$ (present study) and 0.5 M $Na_2SO_4$ (previous work[8]) at pH = 5, clarifying that it is valid for near-neutral sulfates. It was also shown to be active in a slightly alkaline pH up to 8 based on preliminary results. However, the applicability of the mechanism to other environments, for instance, in nitrates, borates, or in highly acidic/alkaline sulfates remain a future topic of investigation. Moreover, if such a salt-film is needed for transpassive film formation in commercially important Ni-Cr-Fe alloys should also be clarified in future studies.

## Conclusions

In this study, we used results of *in situ* Raman spectroscopy measurements and potentiostatic-respirometry in the transpassive regime of Ni in a 0.1 M $K_2SO_4$ at pH =5 to propose a mechanism for transpassive film formation that triggers the oxygen evolution reaction. The key findings of this study are as follows:

- Potentiostatic-respirometry measurements suggest that there is a consistent and significant delay between the moment at which +1.5 $V_{Ag/AgCl}$ was applied and the OER onset.
- *in situ* Raman spectroscopy measurements suggest that the surface film formed on Ni at +1.5 $V_{Ag/AgCl}$ in the transpassive regime is NiOOH.
- Based on the time-delay and Raman spectroscopy results, we suggest the following mechanism for transpassive film formation. It occurs underneath a sulfate salt-film, where the salt-film provides local conditions conducive for the solid-state oxidation of $Ni(OH)_2$ to NiOOH. This mechanism is inspired from the passivation of Fe in acidic sulfate solutions.
- Time resolved Raman spectroscopy reveals a distinct time delay associated with the formation of the transpassive film beneath the possible salt film, and this delay decreases with increasing hold potentials. Moreover, the existence of the time-delay, even when held +1 V above the reversible potential for OER suggests that the salt-film formation is a pre-requisite for secondary passivation and OER onset.
- Preliminary results suggest that the mechanism may hold even at higher pH values.

## Acknowledgments

KH and SV acknowledge technical discussions with Prof. Gerald S. Frankel.

Funding by the Deutsche Forschungsgemeinschaft (DFG, German Research Foundation) Project-ID 517690381 (VI 350/13–1) is acknowledged. (KH and SV)

KH acknowledges the financial support of the Alexander von Humboldt foundation through Humboldt postdoctoral fellowship.

## References

1. L. J. Oblonsky and T. M. Devine, *Journal of The Electrochemical Society*, **142**, 3677 (1995).

2. F. Wang, S. Harrington, and T. M. Devine, *ECS Transactions*, **3**, 39 (2007).

3. H. Su, Y. Ye, K.-J. Lee, J. Zeng, and E. J. Crumlin, *Journal of Physics D: Applied Physics*, **54**, 374001 (2021).

4. Y. Han, S. Axnanda, E. J. Crumlin, R. Chang, B. Mao, Z. Hussain, P. N. Ross, Y. Li, and Z. Liu, *The Journal of Physical Chemistry B*, **122**, 666 (2018).

5. L. J. Oblonsky and M. P. Ryan, *Journal of The Electrochemical Society*, **148**, B405 (2001).

6. A. J. Davenport, M. Sansone, J. A. Bardwell, A. J. Aldykiewicz, M. Taube, and C. M. Vitus, *Journal of The Electrochemical Society*, **141**, L6 (1994).

7. P. Schmuki, S. Virtanen, A. J. Davenport, and C. M. Vitus, *Journal of The Electrochemical Society*, **143**, 3997 (1996).

8. K. Hariharan, A.-K. Bach, M. P. Bruns, and S. Virtanen, *Electrochimica Acta*, 146461 (2025).

9. S. Choudhary, K. Ogle, O. Gharbi, S. Thomas, and N. Birbilis, *Electrochemical Science Advances*, **2**, e2100196 (2022).

10. L. H. Prado, S. Virtanen, N. Weineck, A. Ghicov, and F. Kessler, *Journal of Power Sources*, **613**, 234815 (2024).

11. G. Liu, F. Hou, S. Peng, X. Wang, and B. Fang, *International Journal of Minerals, Metallurgy and Materials*, **29**, 1099 (2022).

12. X. Li, P. Zhou, K. Ogle, S. Proch, M. Paliwal, A. Jansson, and J. Westlinder, *International Journal of Hydrogen Energy*, **45**, 984 (2020).

13. A. Maki, *Saikuru Kiko Giho* (2002).

14. D. N. T. Barton, T. Grebennikova, A. E. Denman, T. Carey, D. L. Engelberg, and C. A. Sharrad, *Journal of Nuclear Materials*, **583**, 154551 (2023).

15. P. Fauvet, in *Nuclear Corrosion Science and Engineering*, D. Féron Editor, p. 679, Woodhead Publishing (2012).

16. P. T. Wilson, N. J. Laycock, M. P. Ryan, D. S. Crouch, and H. S. Isaacs, Transpassive Corrosion of Stainless Steels and Nickel-Base Alloys, in *CAP*, Auckland, NZ (2000).

17. M. Keddam, H. Takenouti, and N. Yu, *Journal of The Electrochemical Society*, **132**, 2561 (1985).

18. M. Datta and D. Landolt, *Journal of the Electrochemical Society*, **124**, 483 (1977).

19. A. Larsson, A. Grespi, G. Abbondanza, J. Eidhagen, D. Gajdek, K. Simonov, X. Yue, U. Lienert, Z. Hegedüs, A. Jeromin, T. F. Keller, M. Scardamaglia, A. Shavorskiy, L. R. Merte, J. Pan, and E. Lundgren, *Advanced Materials*, **35**, 2304621 (2023).

20. P. W. T. Lu and S. Srinivasan, *Journal of The Electrochemical Society*, **125**, 1416 (1978).

21. C. Davidson and S. Srinivasan, *Journal of The Electrochemical Society*, **127**, 1060 (1980).

22. S. Srinivasan, P. Lu, G. Kissel, and F. Kulesa, *Chemical/Hydrogen Energy Systems Contractor Review*, 34 (1978).

23. X. Romero, E. Poussel, and J. M. Mermet, *Spectrochimica Acta Part B: Atomic Spectroscopy*, **52**, 495 (1997).

24. S. Choudhary, K. Marusak, T. Eldred, and R. G. Kelly, *Journal of The Electrochemical Society*, **169**, 111505 (2022).

25. P. GmbH, Oxygen Sensors: Fiber-optic and Contactless, in, PyroScience GmbH, Aachen, Germany (2024).

26. C. Xie, J. Yuan, K. Hariharan, S. Virtanen, J. Han, and K. M. Ogle, *Available at SSRN 5912292*.

27. M. Strebl, M. Bruns, and S. Virtanen, *Journal of The Electrochemical Society*, **167**, 021510 (2020).

28. M. G. Strebl, M. P. Bruns, G. Schulze, and S. Virtanen, *Journal of The Electrochemical Society*, **168**, 011502 (2021).

29. M. G. Strebl, M. P. Bruns, and S. Virtanen, *Journal of The Electrochemical Society*, **170**, 061503 (2023).

30. M. G. Strebl, M. P. Bruns, and S. Virtanen, *Electrochimica Acta*, **412**, 140152 (2022).

31. P. Marcus, J. Oudar, and I. Olefjord, *Materials Science and Engineering*, **42**, 191 (1980).

32. B. MacDougall and M. J. Graham, in *Corrosion mechanisms in Theory and Practice*, p. 198, CRC Press (2002).

33. E. S. Lambers, C. N. Dykstal, J. M. Seo, J. E. Rowe, and P. H. Holloway, *Oxidation of Metals*, **45**, 301 (1996).

34. B. S. Yeo and A. T. Bell, *The Journal of Physical Chemistry C*, **116**, 8394 (2012).

35. C. W. Stone and P. J. Mahon, *Journal of The Electrochemical Society*, **172**, 076504 (2025).

36. N. Boucherit, P. Delichere, S. Joiret, and A. Hugot le Goff, in *Materials Science Forum*, p. 51 (1989).

37. N. Hara and K. Sugimoto, *Transactions of the Japan Institute of Metals*, **24**, 236 (1983).

38. O. E. Barcia, O. R. Mattos, and B. Tribollet, *Journal of The Electrochemical Society*, **139**, 446 (1992).

39. C. A. Melendres and B. S. Tani, *Journal of The Electrochemical Society*, **133**, 1059 (1986).

40. P. Delichere, A. Hugot-Le Goff, and N. Yu, *Journal of The Electrochemical Society*, **133**, 2106 (1986).

41. T. R. Beck, *Journal of the Electrochemical Society*, **129**, 2412 (1982).

42. H. L. Le Chatelier, *Comptes rendus*, **99**, 786 (1884).

43. M. Iida and T. Ohtsuka, *Corrosion Science*, **49**, 1408 (2007).

**Figures and Figure captions**

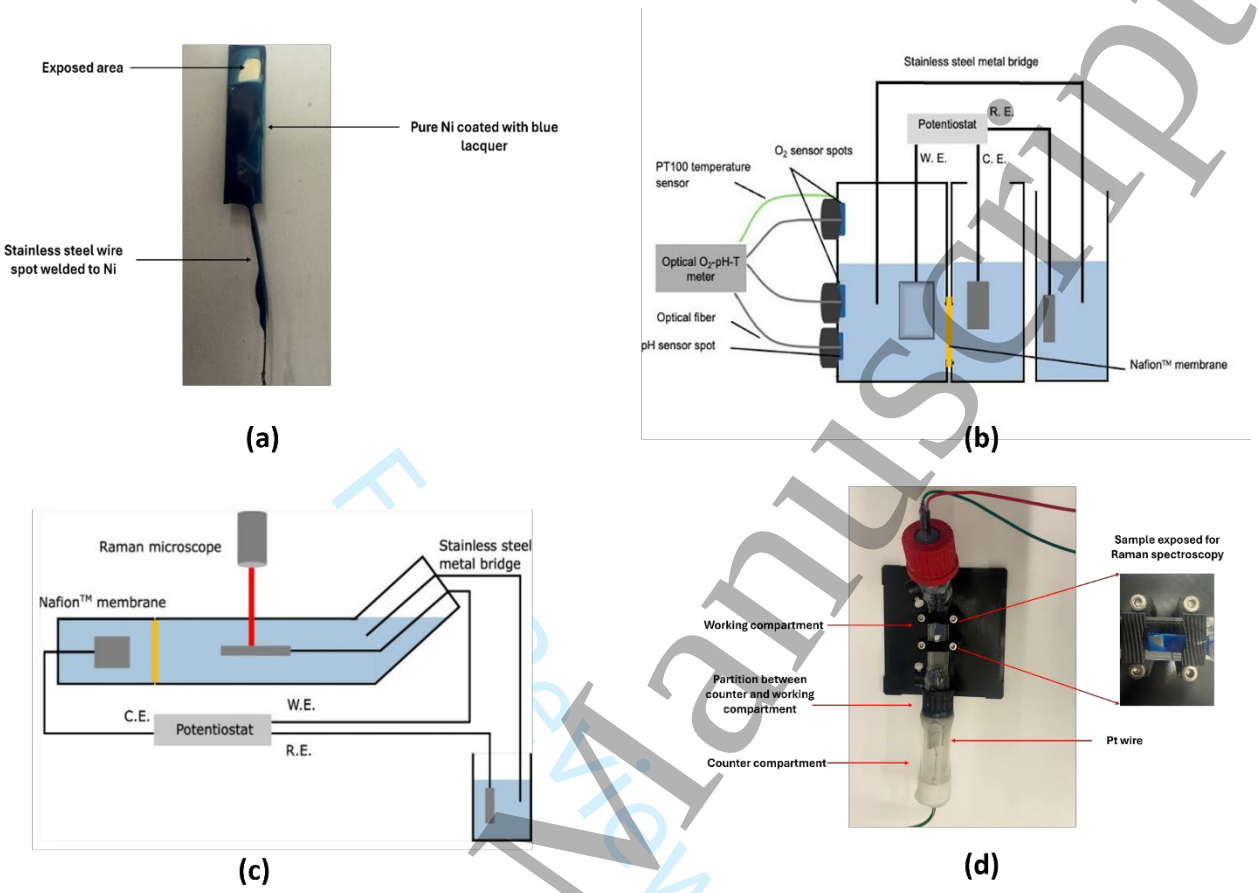


**Figure 1** – (a) Typical Ni sample used for in-situ Raman spectroscopy and electrochemical measurements coated with blue lacquer, (b) Electrochemical-Respirometric setup used for standalone experiments (Reproduced from Hariharan et al.[8] – originally published under CC BY-NC 4.0), (c) Schematic of the electrochemical cell used for Raman spectroscopy measurements, (d) The electrochemical cell designed for Raman spectroscopy measurements along with the positioning of the specimen for the measurement.

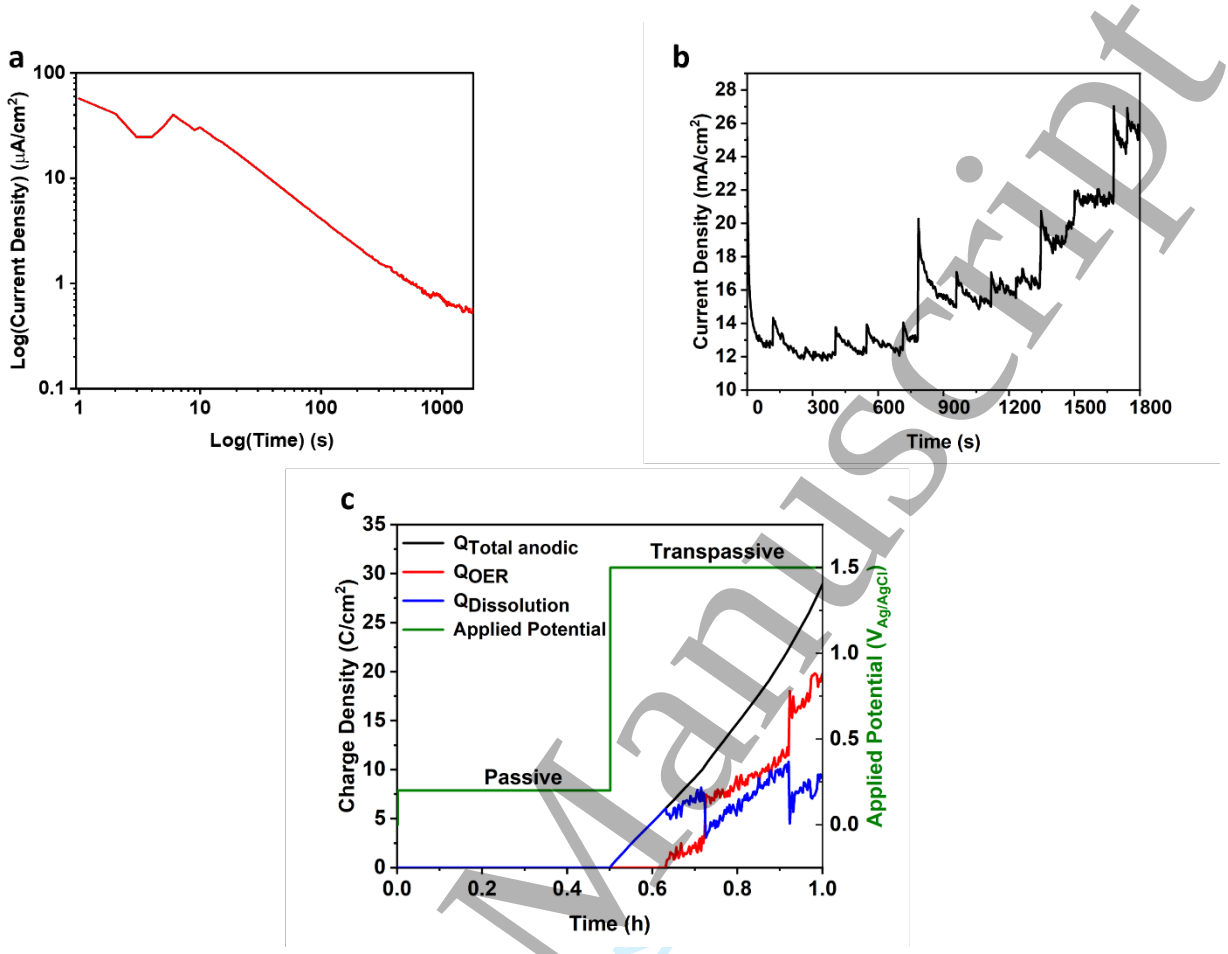


**Figure 2** – (a) Log current density vs. log time plot during passive hold at +0.2 $V_{Ag/AgCl}$, (b) Current density vs. time plot during transpassive hold at +1.5 $V_{Ag/AgCl}$, (c) Charge density vs. time plot showing oxygen evolution (measured with respirometry) and metal dissolution (inferred).

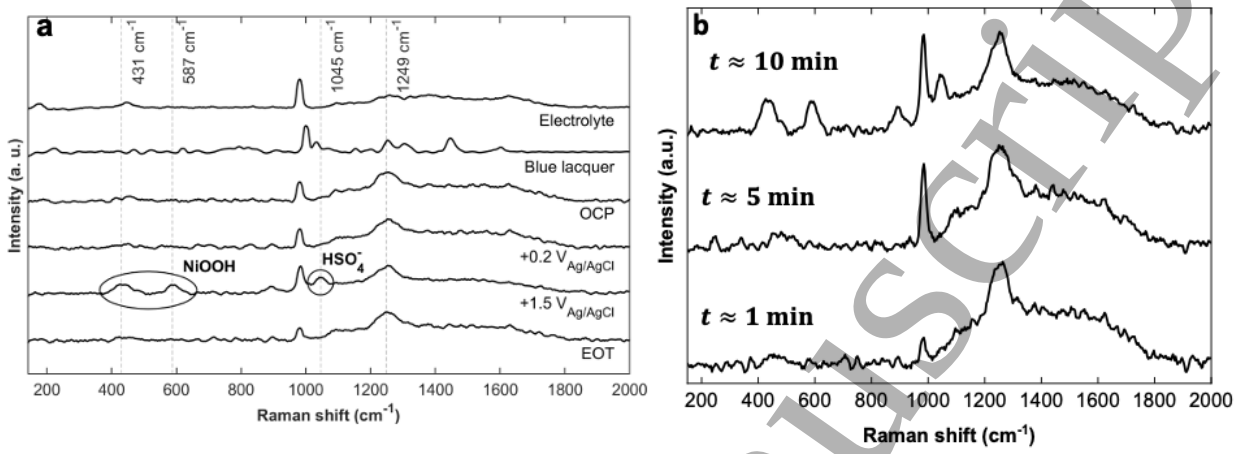


**Figure 3** – (a) Raman spectra (785 nm laser) collected under different electrochemical conditions, also showing the spectra of the electrolyte before the measurement and outside of the Raman setup, and the blue lacquer covering the sample surface outside of the region of interest (b) Time resolved Raman spectra during the +1.5 $V_{Ag/AgCl}$ hold.

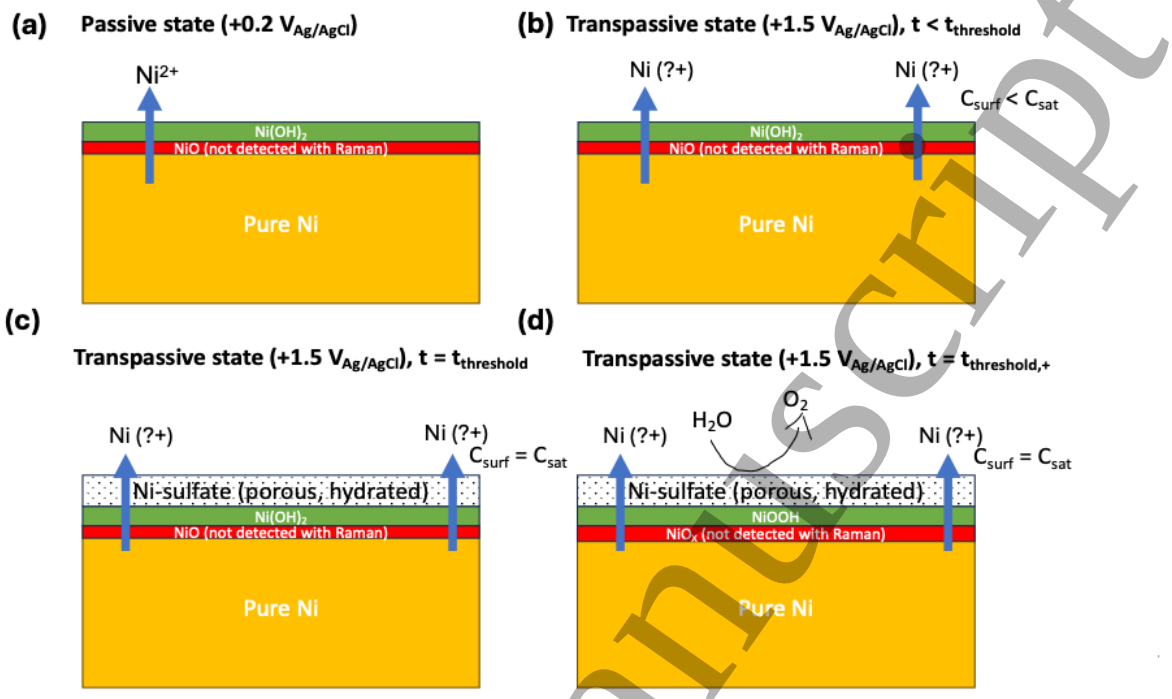


**Figure 4** – Schematic representing the processes occurring on Ni surface exposed to 0.1 M $K_2SO_4$ at (a) OCP and 0.2 $V_{Ag/AgCl}$, (b) +1.5 $V_{Ag/AgCl}$ ($t < t_{threshold}$) before salt-film formation, (c) +1.5 $V_{Ag/AgCl}$ ($t = t_{threshold}$) at the time of salt-film formation, (d) +1.5 $V_{Ag/AgCl}$ ($t = t_{threshold,+}$) moments after salt-film formation.

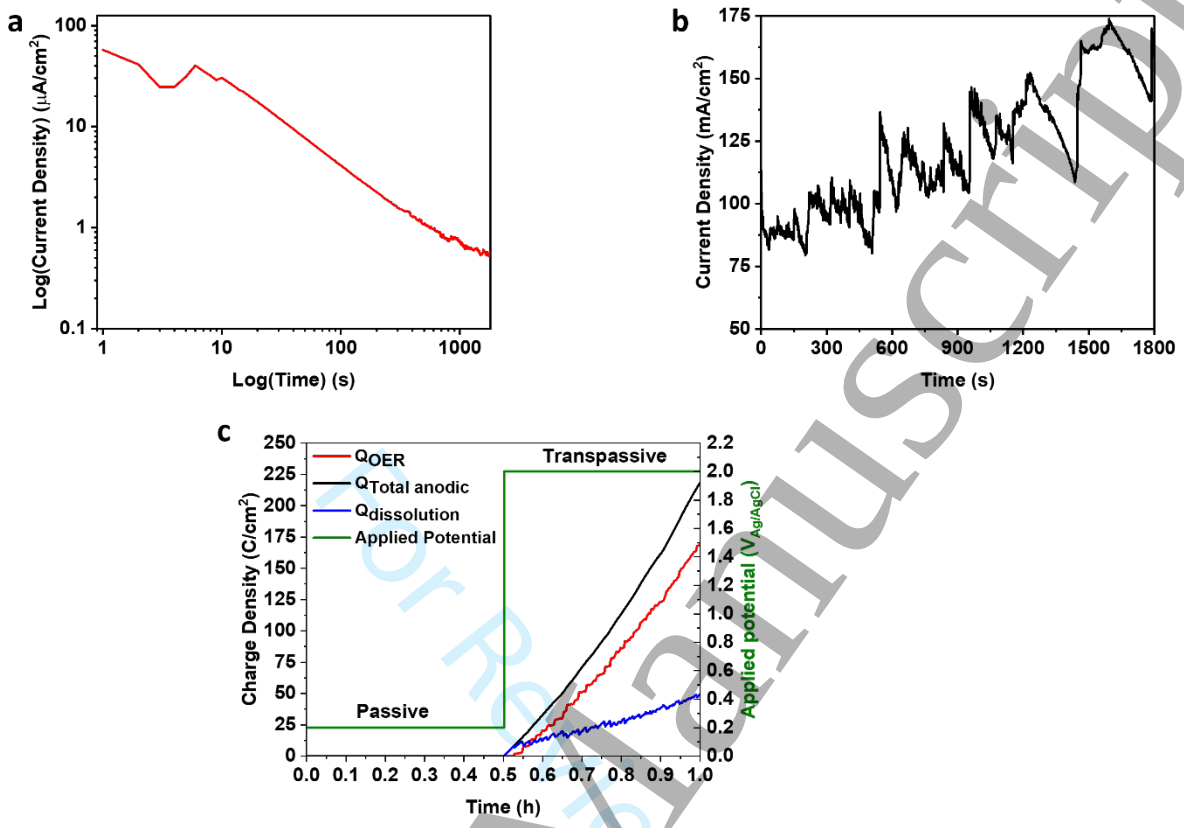


**Figure 5** – (a) Log current density vs. log time plot during passive hold at +0.2 $V_{Ag/AgCl}$, (b) Current density vs. time plot during transpassive hold at +2 $V_{Ag/AgCl}$, (c) Charge density vs. time plot showing oxygen evolution (measured with respirometry) and metal dissolution (inferred).

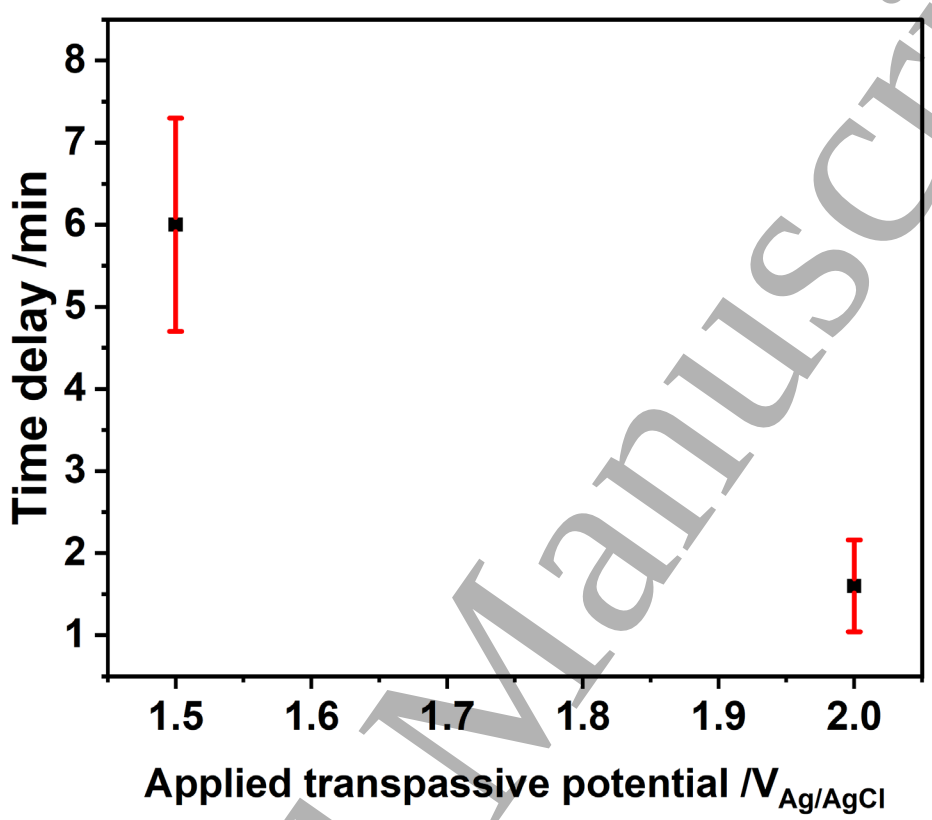


**Figure 6** – Time-delay for secondary passivation/OER onset as a function of applied transpassive hold potential, showing a decreasing trend with increase in hold potential. The error bars indicate the standard deviation of three repetitions.